

Dynamic spin-Hall effect and driven spin helix for linear spin-orbit interactions

Mathias Duckheim¹, Dmitrii L. Maslov², and Daniel Loss¹

¹*Department of Physics, University of Basel, CH-4056 Basel, Switzerland, and*

²*Department of Physics, University of Florida, Gainesville, FL 32611-8440, USA*

(Dated: November 28, 2018)

We derive boundary conditions for the electrically induced spin accumulation in a finite, disordered 2D semiconductor channel. While for DC electric fields these boundary conditions select spatially constant spin profiles equivalent to a vanishing spin-Hall effect, we show that an in-plane ac electric field results in a non-zero ac spin-Hall effect, i.e., it generates a spatially non-uniform out-of-plane polarization even for linear intrinsic spin-orbit interactions. Analyzing different geometries in [001] and [110]-grown quantum wells, we find that although this out-of-plane polarization is typically confined to within a few spin-orbit lengths from the channel edges, it is also possible to generate spatially oscillating spin profiles which extend over the whole channel. The latter is due to the excitation of a driven spin-helix mode in the transverse direction of the channel. We show that while finite frequencies suppress this mode, it can be amplified by a magnetic field tuned to resonance with the frequency of the electric field. In this case, finite size effects at equal strengths of Rashba- and Dresselhaus SOI lead to an enhancement of the magnitude of this helix mode. We comment on the relation between spin currents and boundary conditions.

PACS numbers: 72.25.Dc 85.75.-d, 75.80.+q

I. INTRODUCTION

Electron systems with spin-orbit interaction show a variety of spin-electric effects arising from the coupling between (orbital) charge and spin degrees of freedom. The most prominent examples are the spin-Hall effect^{1,2,3,4} and current induced spin polarization^{5,6,7}, both of which have received substantial interest due to their potential to generate and control spin polarization with electric fields. This type of electrical control is a prerequisite for integrating spin effects into standard lithographic semiconductor structures and, ultimately, utilizing the spin degree of freedom as a carrier of information.⁸

The spin-Hall effect (SHE) manifests itself experimentally^{2,3,9} as current induced spin polarization (CISP) at the edges of a Hall-bar (in the absence of a magnetic field). Initial theoretical studies of the SHE¹⁰ in 2D electron systems have focused on linear intrinsic Rashba- and/or Dresselhaus spin-orbit interaction (SOI) and interpreted this boundary spin accumulation in terms of a spin current¹ (defined as a symmetrized product of spin and current densities) flowing transverse to the applied electric field. However, these arguments have been plagued by ambiguities, such as equilibrium spin currents¹¹ and the absence of spin conservation^{12,13} in systems with intrinsic SOI. Explicit diagrammatic calculations^{13,14,15} for disordered systems and a more general, non-perturbative argument^{12,13,16} show that the spin-current is absent in systems with standard linear-in-momentum SOI.^{5,8}

A more straightforward approach is to calculate the quantity directly measured in experiments: the spatially and time resolved spin density.^{17,18,19} In weakly disordered systems with $E_F \gg \tau^{-1}, \Delta_{\text{SO}}$ (where E_F is the Fermi energy, τ the momentum relaxation time, and Δ_{SO} the spin-orbit splitting) the spin density is described

by spin diffusion equations derived in Keldysh^{20,21,22} or density matrix approaches.^{19,23,24} These equations have been used to study various effects, such as the response to an electromagnetic wave,²⁵ spin currents,²⁰ spin relaxation,^{26,27} boundary spin accumulation for dc^{17,18,19,28,29} and abruptly switched^{30,31} electric fields, and more general interface problems.^{22,24}

A significant difference between charge and spin diffusion, as described by these equations, is the existence of spatially oscillating spin density modes. For instance, a gradient of the out-of-plane spin density acts as a torque on the in-plane spin and vice versa, leading to a periodic spatial modulation of both in- and out-of-plane spin densities with a period given by the spin-orbit length λ_{SO} . General solutions of the spin diffusion equations are damped spatial spin density oscillations with a period given by the spin-orbit relaxation length λ_{SO} . An example of such periodic modes in diffusive systems was first described in Ref. 32 (see, in particular, Eq. (7) there) for the case of equal strengths of the Rashba and linear Dresselhaus SOI. For this particular case and in the absence of the cubic SOI, these modes are long-lived and static and are thus referred to as persistent spin helix.²¹ Modes of this type have recently been observed.³³

However, when analyzing these equations for a specific geometry, e.g., in a narrow channel for the case of the SHE, the weight of these oscillatory modes in the solution is determined by boundary conditions (BCs). For instance, assuming vanishing polarization at the boundary one obtains an oscillatory behavior of the spin density,²⁸ resembling the spin profile measured in Ref. 3. On the other hand, for a von-Neumann boundary condition (vanishing normal gradient of the polarization), the spin profile is spatially uniform. Thus, the existence of the SHE depends crucially on the BCs. This circumstance motivated a number of studies where BCs for sys-

tems with SOI were derived microscopically, both in the diffusive^{17,19,22,28,29} and ballistic³⁴ regimes.

It has been shown^{22,29} that BCs (for hard-wall spin-conserving boundaries) in disordered⁵⁹ systems with linear SOI and for dc electric fields require the spin density to be equal to its value in the bulk, i.e., far away from the boundary, and, thus, lead to a spatially uniform spin profile. This null result is consistent with zero spin currents.^{13,14,15,16,20} The experimentally observed dc spin accumulation³ in 2DEGs thus requires an explanation accounting for both extrinsic^{35,36} and (cubic¹⁸) intrinsic effects. That a spin current is finite at finite frequencies and for linear SOIs,^{20,37,38} however, hints at the presence of boundary spin accumulation in ac solutions. In this article, we focus on the intrinsic mechanism, and show that a *dynamic* SHE, i.e., boundary spin polarization induced by an ac voltage, is present even in a minimal intrinsic model.

The dynamic SHE arises due to the excitation of spatially non-uniform spin diffusion modes. In the Hall-bar geometry, these modes are excited by a spatially uniform ac electric field and lead to accumulation and spatial oscillations of the spin density close to the boundaries. Analyzing these modes as a function of SOI strengths and in the presence of an external, in-plane magnetic field, we find a spin diffusion mode which is a finite-frequency analog of the persistent spin helix.^{21,27,32,33} The relaxation length of this mode -while finite for generic linear SOIs- becomes infinite when the Rashba and Dresselhaus SOI strengths are equal and when the magnetic field is tuned to resonance with the frequency of the electric field. This particularly robust mode, originating from electric-dipole-induced spin resonance (EDSR),^{39,40,37,38,41,42,43,44,45} gives rise to a spatially oscillating spin profile which extends infinitely far away from the Hall-bar boundary. This driven spin helix has the same spatial oscillation period as the persistent spin helix^{21,32,33} but, whereas the latter is static, the former oscillates in time at the frequency of the applied bias. The prediction of a driven spin helix is one of the main results of this paper.

Using a linear response approach, we solve the problem of a hard-wall boundary in a disordered 2D electron gas in the presence of an ac electric field. The derivation of the BCs is similar to the one in Refs. 19 and 29. We find that while the bulk polarization is reduced at finite frequencies, the BCs require the polarization at the boundary to have a larger value. The spin polarization is, thus, no longer spatially uniform: there is a spin accumulation at the boundary and spatial oscillations decaying towards the bulk of the sample. The amplitude of this spatial oscillations at frequency ω is proportional to ω/Γ , where Γ is the Dyakonov-Perel spin relaxation rate. Since typically $\Gamma \ll \tau^{-1}$, where τ is the transport time, the dynamic SHE becomes pronounced even for frequencies $\omega\tau \ll 1$. Analyzing different geometries and SOIs, we find that it is possible to excite a predominantly oscillatory mode for equal strength of the Rashba and

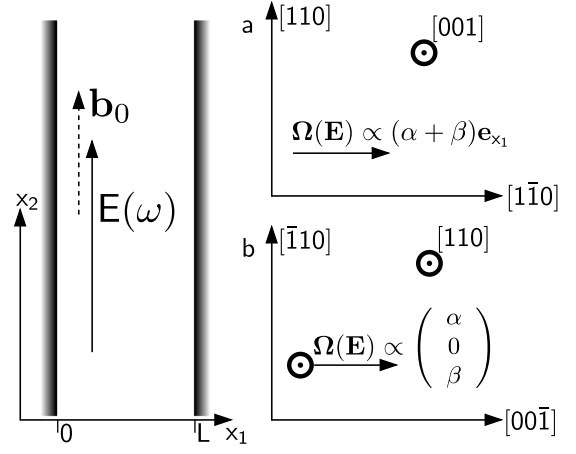


FIG. 1: Left: Conducting channel infinite in the \mathbf{e}_{x_2} -direction and of width L in the \mathbf{e}_{x_1} direction. ac Electric field $\mathbf{E}(\omega) \parallel \mathbf{e}_{x_2}$ induces boundary spin accumulation. An external magnetic field \mathbf{b}_0 , applied parallel to \mathbf{E} , gives rise to EDSR (see Sec. VII). Right, (a): a “standard” [001]-grown quantum well with the [110] crystal axis taken along the x_2 -direction. The bulk polarization $\Omega(\mathbf{eE}\tau) \propto \mathbf{e}_{x_1}(\alpha + \beta)$ points along \mathbf{e}_{x_1} [cf. Eqs. (2) and (3)]. Right, (b): a [110]-grown quantum well with $\mathbf{E} \parallel [\bar{1}10]$ along \mathbf{e}_{x_2} . The internal field [see Eq. (4)] $\Omega(\mathbf{eE}\tau)$ has both in-plane (due to the Rashba SOI) and out-of-plane (due to the Dresselhaus SOI) components.

Dresselhaus SOI –a driven spin helix described above.

The paper is organized as follows. In Sec. II, we introduce our model and formulate the linear response formalism for SHE. In Sec. III, we sketch the derivation of the integral equation for the spin density, which is then used to derive the diffusion equation and its boundary conditions. (A more detailed derivation is deferred to appendix A.) In Sec. IV, we derive boundary conditions in the presence of ac electric field and comment on the relation between spin currents and these boundary conditions in Sec. V. In Sec. VI we calculate the spatially resolved spin profiles at finite frequencies in various geometries in [001]- and [110]-grown quantum wells. Generation of a driven spin helix under the conditions of EDSR is discussed in Sec. VII.

II. PRELIMINARIES

We consider a disordered 2DEG confined to a quantum well (QW) channel of width L (see Fig. 1) with non-interacting electrons of mass m and charge e . The system is described by the Hamiltonian

$$H = \frac{\mathbf{p}^2}{2m} + \Omega(\mathbf{p}) \cdot \boldsymbol{\sigma} + \mathbf{b}_0 \cdot \boldsymbol{\sigma} + V. \quad (1)$$

Here, $\mathbf{p} = (p_1, p_2, 0)$ is the in-plane momentum, $\Omega(\mathbf{p})_i = \Omega_{ij}p_j$ is a linear, vector-valued function of \mathbf{p} describing spin-orbit interaction, $2\mathbf{b}_0 = g\mu_B(B_1, B_2, 0)$ is a magnetic field (equal in magnitude to the Zeeman energy)

applied parallel to the 2DEG, and $\sigma = (\sigma^1, \sigma^2, \sigma^3)$ are the Pauli matrices (and $\sigma^0 = \mathbb{1}$). The disorder potential V due to static short-ranged impurities randomly distributed over the channel is characterized by the mean free path $l = \tau p_F / m$, where τ is the scattering time and p_F is the Fermi momentum.

We calculate the impurity-averaged, spatially-dependent spin density $\hat{S}^i(\mathbf{r}) = \sigma^i \delta(\mathbf{r} - \hat{\mathbf{x}})$ due to in-plane ac electric field $\mathbf{E}(\omega) = \mathbf{E}_0 \delta(\omega - \omega_0)$. As it will be shown below, the overall magnitude of \mathbf{S} is determined by the bulk spin polarization due to CISP far away from the boundary. We therefore briefly discuss CISP in different geometries. We define the nominal polarization

$$\mathbf{S}_b \equiv -\nu 2\Omega(e\mathbf{E}(\omega)\tau), \quad (2)$$

(with $\nu = m/2\pi$ being the density of states per spin) which at zero frequency ($\omega_0 = 0$) coincides with the bulk polarization.⁶ In this case, \mathbf{S}_b is simply a paramagnetic spin response to an effective magnetic field $\Omega(e\mathbf{E}_0\tau)$. The latter is the internal field due to the electrically induced drift momentum $e\mathbf{E}\tau$ and SOI.

Both the magnitude and direction of \mathbf{S}_b depend on the SOI mechanism. We consider two cases (see Fig. 1): the “standard” [001]- and [110]-grown QW. The Rashba SOI (with strength α) due to an asymmetry in the confinement potential has the same form in both cases and is assumed to be tunable. The Dresselhaus induced fields $\Omega_{D,[001]}$, $\Omega_{D,[110]}$ are in-plane and out-of-plane in the [001] and [110]-grown QWs, respectively. For convenience, we define $\xi_\alpha = 2\alpha p_F \tau$, $\xi_\beta = 2\beta p_F \tau$ as the ratios of the mean free path and spin precession length due the Rashba and Dresselhaus SOIs, respectively. The vector couplings of the SOIs are described by

$$\Omega_{[001]} = \begin{pmatrix} 0 & \alpha + \beta & 0 \\ -(\alpha - \beta) & 0 & 0 \\ 0 & 0 & 0 \end{pmatrix} \quad (3)$$

for case (a) in Fig. 1 and

$$\Omega_{[110]} = \begin{pmatrix} 0 & \alpha & 0 \\ -\alpha & 0 & 0 \\ 0 & \beta & 0 \end{pmatrix} \quad (4)$$

for case (b). In case (a), the bulk polarization $S_b \propto -\mathbf{e}_{x_1}(\alpha + \beta)$ points along the (negative) x_1 -axis. When the Rashba- and Dresselhaus SOIs are of comparable strength, i.e., $\alpha \approx +\beta$ (or $\alpha \approx -\beta$), constructive (destructive) interference between the two SOI mechanisms occurs.³² In this case, one spin component [along x_1 (x_2)] becomes conserved. A similar situation occurs in the [110]-grown QW, where the out-of-plane spin is conserved if the Rashba SOI is relatively small. Here the bulk polarization points out-of-plane and is, thus, easier accessible in optical measurements.^{2,3,45}

The induced spin density $S^\mu(\mathbf{r})$ is described by coupled spin diffusion equations^{18,20,23} which can be derived in

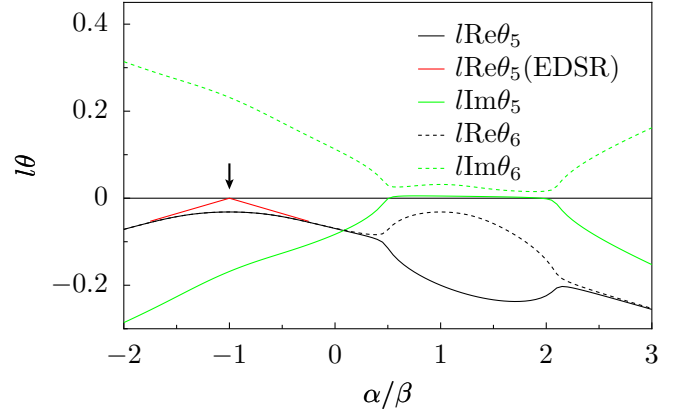


FIG. 2: (color online) Characteristic wave numbers θ of the homogeneous solutions $s_5(r_1) = s_{5,0}e^{\theta_5 r_1}$ and $s_6 = s_{6,0}e^{\theta_6 r_1}$ of Eq. (7) as a function of α/β for $\omega\tau = 10^{-3}$ and $\xi_\beta = 0.1$ in a [001]-grown quantum well. For $\alpha = -\beta$ (indicated by arrow), the wave numbers have small real parts $|\text{Re}\theta_5| \approx |\text{Re}\sqrt{-2i\omega\tau}| \ll 1$, which implies a nearly undamped oscillatory mode. Under EDSR conditions, $\text{Re}\theta_5$ vanishes identically at $\alpha + \beta = 0$ [cf. Eq. (32)]. The presence of modes with almost imaginary wave numbers leads to an oscillating spin profile, as shown in Fig. 3.

the Keldysh^{20,21,22} or density matrix formalisms.^{19,23,24} As a starting point for the derivation of the boundary conditions, we present here an alternative derivation based on a diagrammatic linear response approach. The detailed derivation is deferred to Appendix A. We obtain an integral equation for the spin density

$$S^i(\mathbf{r}) - S_b^i = i\omega\tau S_b^i + \int d^2x X^{ij}(\mathbf{r}, \mathbf{x})(S^j(\mathbf{x}) - S_b^j) \quad (5)$$

valid in the regime $1/E_F\tau \ll 1$, where

$$X^{\mu\nu}(\mathbf{r}, \mathbf{x}) = \frac{1}{2m\tau} \text{tr} \{ \sigma^\mu G_{E_F+\omega}^R(\mathbf{r}, \mathbf{x}) \sigma^\nu G_{E_F}^A(\mathbf{x}, \mathbf{r}) \}. \quad (6)$$

Here, E_F is the Fermi energy, $\text{tr}\{\dots\}$ denotes the trace over spin s , $\hat{v}_j = \frac{\hat{p}_j}{m} + \Omega_{kj}\sigma^k$ is the velocity operator containing a spin-dependent term, and $G_E^{R/A}$ the impurity-averaged, retarded/advanced Green functions at energy E . Note that for $\omega = 0$ the integral equation (5) depends only on the combination $\mathbf{S} - \mathbf{S}_b$ so that the spatially uniform solution $\mathbf{S} = \mathbf{S}_b$ is immediate. The uniform spin profile is equivalent to the absence of the SHE, whose presence would cause a spatial modulation of S at the boundary.

III. DIFFUSION EQUATION

Far from the sample boundary, the impurity-averaged Green functions and, hence, the kernel $X^{\mu\nu}(\mathbf{r}, \mathbf{x}') \approx e^{-|\mathbf{r}-\mathbf{x}'|/l}$ in Eq. (5) decay on the scale of the mean free path l , which is the shortest length scale of the diffusion problem. The behavior of S on scales larger than l

can, thus, be found by expanding: $\mathbf{S}(\mathbf{x}) \approx \mathbf{S}(\mathbf{r}) + (\mathbf{x} - \mathbf{r})_i \partial_{r_i} \mathbf{S}(\mathbf{r}) + \frac{1}{2} (\mathbf{x} - \mathbf{r})_k (\mathbf{x} - \mathbf{r})_l \partial_{r_k} \partial_{r_l} \mathbf{S}(\mathbf{r})$. In this way, one obtains the coupled spin diffusion equation

$$[-i\omega + \Gamma - D\Delta_{\mathbf{r}}](\mathbf{S}(\mathbf{r}) - \mathbf{S}_b) - 2[\mathbf{b} - p_F \mathbf{\Omega}(l\nabla_r)] \times (\mathbf{S}(\mathbf{r}) - \mathbf{S}_b) = i\omega \mathbf{S}_b, \quad (7)$$

where $D = v_F l/2$ is the diffusion constant and $\Gamma^{ij} = [\text{tr}\{(\Omega\Omega^T)\}\delta_{ij} - (\Omega\Omega^T)_{ij}]2p_F^2\tau$ is the spin relaxation tensor.

We now apply Eq. (7) to the two specific geometries in Fig. 1 (a) and (b). Assuming translational invariance along \mathbf{e}_{x_2} , we find for the [001]-grown QW with $\mathbf{E}||[110]||\mathbf{e}_{x_2}$

$$[-i\omega - D\partial_{r_1}^2 + \Gamma_-](S^1 - S_b) + C_- \partial_{r_1} S^3 = i\omega S_b, \quad (8)$$

$$[-i\omega - D\partial_{r_1}^2 + \Gamma_+](S^2 - S_b) = 0, \quad (9)$$

$$[-i\omega - D\partial_{r_1}^2 + \Gamma_+ + \Gamma_-](S^3 - S_b) - C_- \partial_{r_1} S^1 = 0, \quad (10)$$

where $\Gamma_{\pm} = 2p_F^2\tau(\alpha \pm \beta)^2$, $C_{\pm} = 2p_F l(\beta \pm \alpha)$, $\omega_L = 2b_0$ and $S_b = -2\nu e E \tau(\alpha + \beta)$.

In case (b) of a [110]-grown QW with $\mathbf{b}_0, \mathbf{E}||[\bar{1}10]||\mathbf{e}_{x_2}$ we find

$$[-D\partial_{r_1}^2 - i\omega + \Gamma'_1 + \Gamma'_2](S^1 - S_b^1) - [C'_2 \partial_{r_1} + \omega_L + \sqrt{\Gamma'_1 \Gamma'_2}](S^3 - S_b^3) = i\omega S_b^1, \quad (11)$$

$$[-D\partial_{r_1}^2 - i\omega + \Gamma'_1 + \Gamma'_2]S^2 = 0, \quad (12)$$

$$[-D\partial_{r_1}^2 - i\omega + 2\Gamma'_2](S^3 - S_b^3) + [C'_2 \partial_{r_1} + \omega_L - \sqrt{\Gamma'_1 \Gamma'_2}](S^1 - S_b^1) = i\omega S_b^3, \quad (13)$$

where $S_b^1 = -2\nu e E \tau(\alpha, 0, \beta)$, $\Gamma'_1 = 2p_F^2\tau\beta^2$, $\Gamma'_2 = 2p_F^2\tau\alpha^2$, $C'_1 = p_F l\beta$, $C'_2 = p_F l\alpha$, and $\omega_L = 2b_0$. Note that in this geometry the Dresselhaus SOI adds to \mathbf{S}_b , whereas for $\mathbf{E}||[001]$ the electric field does not couple to the Dresselhaus term.⁴⁶

IV. BOUNDARY CONDITIONS

The diffusion equation (7) has to be supplemented with boundary conditions. These match the bulk solutions of the diffusion equation (7) with the solution of the integral equation Eq. (5) in the region $1/p_F \ll x_1 \ll l$ close to the boundary. Here, we follow the approach used in Refs. 19 and 29. We choose $x_1 = 0$ as the boundary and construct the impurity-averaged Green functions $G^{R/A}(\mathbf{x}, \mathbf{x}')$ which satisfy the Dyson equation $\langle \mathbf{x} | [(\omega - \hat{H}_0 - \hat{H}_{SO} - \hat{\Sigma})\hat{G}] | \mathbf{x}' \rangle = \delta(\mathbf{x} - \mathbf{x}')$ with H_0 being the Hamiltonian in the absence of SOI and $\hat{\Sigma}$ being the self-energy due to impurity scattering.^{47,48} We, moreover, impose the hard-wall, spin-conserving boundary conditions $G(\mathbf{x}, \mathbf{x}')|_{x_1, x'_1=0} = 0$ for either argument at the boundary.

To 0th order in the SOI, these conditions are satisfied by image constructions $G_0^{R/A} = G_{b,0}^{R/A} - G_{b,0}^{*R/A}$, where $G_{b,0}^{R/A}$ is the impurity-averaged Green function in the

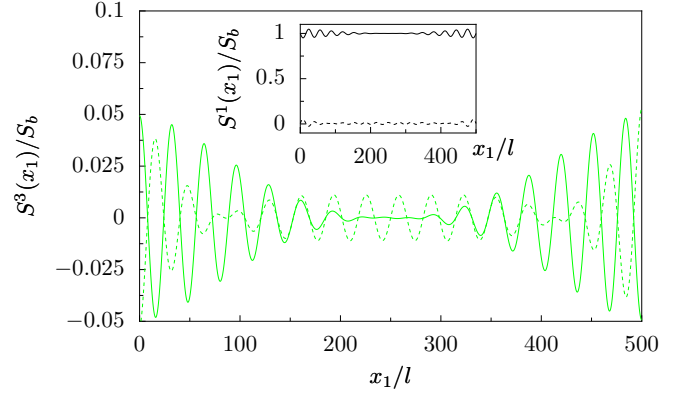


FIG. 3: (color online) Real (solid line) and imaginary parts (dashed line) of the out-of-plane spin density $S^3(x)/S_b$ [solution of Eqs. (8)-(10), (19)] in the standard QW (Fig. 1 a) are shown for $\omega\tau = 10^{-4}$, $\xi_\alpha = 0.1$, $\xi_\beta = -0.095$, and $L = 500l$. As Rashba- and Dresselhaus SOI interfere destructively for this case, the bulk polarization is much smaller than the value discussed in Sec. VI: all other parameters being equal, $S_b = 0.005 \mu\text{m}^{-2}$ instead of $1.1 \mu\text{m}^{-2}$. Inset: In-plane polarization $S^1(x)$ (along the internal field $\mathbf{\Omega}(e\mathbf{E}\tau)$) in the same situation.

bulk and $G_b^{*R/A}(\mathbf{x}, \mathbf{x}') = G_b^{R/A}(\mathbf{x}, (-x'_1, x'_2))$ is the Green function mirror-reflected at the boundary. Neglecting Friedel oscillations of the self-energy at the boundary, which fall off as $1/\sqrt{p_F x_1}$, the Green functions $G^{R/A}$ constructed in this way satisfy the Dyson equation to leading order in $1/E_F\tau$.

To 1st order in H_{SO} the Green functions is found as $\hat{G}_1 = \hat{G}_0 \hat{H}_{SO} \hat{G}_0$. By construction, $G(\mathbf{x}, \mathbf{x}') = [G_0 + G_1](\mathbf{x}, \mathbf{x}')$ satisfies the boundary conditions and the Schrodinger equation to linear order in the spin-orbit interaction. Performing a Fourier transform of the Green function $G(\mathbf{x}, \mathbf{x}') = \int dp_2 G(x_1, x'_1 | p_2) e^{ip_2(x_2 - x'_2)} / (2\pi)$ along the boundary, we find

$$G_0^{R/A}(x_1, x'_1 | p_2) = \frac{\mp i m}{p_E^\pm} \left[e^{\pm i p_E^\pm |x_1 - x'_1|} - e^{\pm i p_E^\pm (x_1 + x'_1)} \right], \quad (14)$$

where $p_E^\pm = \sqrt{2m(E \pm i/2\tau - p_2^2/2m)}$ with p_2 being the momentum along the channel. To first order in H_{SO} , we find

$$G_1^{R/A}(x_1, x'_1 | p_2) = \frac{\mp m^2 \Omega_{k1} \sigma^k}{p_E^\pm} (x_1 - x'_1) \times \left[e^{\pm i p_E^\pm |x_1 - x'_1|} - e^{\pm i p_E^\pm (x_1 + x'_1)} \right] + \dots, \quad (15)$$

where the dots stand for additional terms that do not contribute to the integrals below since they are odd in the longitudinal momentum p_2 .

We are now in a position to derive boundary conditions using the Green functions from Eqs. (14) and (15). We take the limit $\mathbf{r} \rightarrow 0$ of Eq. (5) and expand $\mathbf{S}^i(\mathbf{x}) \approx$

$\mathbf{S}^i(\mathbf{r}) + (x_j - r_j) \frac{\partial}{\partial r_j} \mathbf{S}^i(\mathbf{r})$ in the integrand. This yields

$$0 = i\omega\tau \mathbf{S}_b + (B - 1)(\mathbf{S}(0) - \mathbf{S}_b) + C_j \frac{\partial}{\partial r_j} \mathbf{S}(0), \quad (16)$$

where the coefficients

$$B^{\mu\nu} = \int_{x'_1 > 0} dx'_1 dx'_2 X^{\mu\nu}(\mathbf{x}, \mathbf{x}')|_{x \rightarrow 0} \quad (17)$$

$$C_j^{\mu\nu} = \int_{x'_1 > 0} dx'_1 dx'_2 X^{\mu\nu}(\mathbf{x}, \mathbf{x}')(x'_j - x_j)|_{x \rightarrow 0} \quad (18)$$

are obtained from the spin-spin correlation function $X^{\mu\nu}$ in Eq. (6) evaluated with the Green's functions satisfying the boundary conditions. In symbolic notations, $X \propto G_{b,0}^R G_{b,0}^A + G_{b,0}^{*R} G_{b,0}^{*A} - G_{b,0}^R G_{b,0}^A - G_{b,0}^{*R} G_{b,0}^{*A}$. Note that for $\omega = 0$ the diffusion equation Eq. (7) and the boundary conditions Eq. (16) depend only on the combination $\mathbf{S} - \mathbf{S}_b$, so that the spatially constant solution $\mathbf{S} = \mathbf{S}_b$ is immediate. In particular, there is no spin accumulation close to the boundary in that case in agreement with the literature on the linear intrinsic spin-Hall effect.^{13,14,15,18}

When calculating the spin-spin correlation function $X^{\mu\nu}$ one encounters mixed terms of the form GG^* , which oscillate as a function of x_1 with a period of $1/p_F$. To determine S on length scales larger than l , we neglect these oscillations. This way, we find the BCs

$$l\partial_{\hat{\mathbf{n}}} S^i = -2p_F\tau\Omega(\hat{\mathbf{n}})_m \epsilon_{mij} (S^j - S_b^j), \quad (19)$$

where $\hat{\mathbf{n}}$ is a unit vector normal to the boundary and where we have neglected terms proportional to $\omega\tau \ll 1$.

V. SPIN CURRENT

In this section, we show that a definition of the spin current in terms of an SU(2)-covariant derivative is consistent with both the boundary conditions and the diffusion equation. This definition is equivalent to defining the spin current as the commutator – in contrast to the conventionally used *anticommutator* – of spin and velocity. To see this, we define a Hermitian spin current operator as follows

$$\begin{aligned} \hat{J}_i^\eta(\hat{\mathbf{S}}) &= -\mathcal{D}_i \hat{S}^\eta(\mathbf{r}) = -i[m\hat{v}_{SO,i}, \hat{S}^\eta(\mathbf{r})] \\ &= \frac{\partial}{\partial r_i} \hat{S}^\eta(\mathbf{r}) + 2m\Omega_{ki}\epsilon_{k\eta\eta'} \hat{S}^{\eta'}(\mathbf{r}), \end{aligned} \quad (20)$$

where we have introduced the covariant derivative⁴⁹ $\mathcal{D}_i \cdot = \partial/\partial \hat{x}_i \cdot - i[\mathcal{A}, \cdot]$ with the non-abelian gauge potential $\mathcal{A}_i = -m\Omega_{ki}\sigma^k$ and $\hat{S}^\eta(\mathbf{r}) = \sigma^\eta \delta(\mathbf{r} - \hat{\mathbf{x}})$ is the spin density operator. [Note that \hat{J}_i^η differs by a factor of mass m from the conventionally defined product of velocity and spin.] From Eq. (20) we obtain a spin current J by replacing $\hat{\mathbf{S}}$ by $\mathbf{S}(\mathbf{r}) - \mathbf{S}_b$ in the second line of Eq. (20), i.e.,

$$J_i^\eta(\mathbf{r}) = -\mathcal{D}_i^{\eta\eta'} (S^{\eta'}(\mathbf{r}) - S_b^{\eta'}), \quad (21)$$

where $-\mathcal{D}_i^{\eta\eta'} = \delta^{\eta\eta'} \partial/\partial r_i + 2m\Omega_{ki}\epsilon_{k\eta\eta'}$. The BCs in Eq. (19) are then equivalent to the requirement that the normal component of \mathbf{J} vanishes at the boundary, i.e., $\hat{\mathbf{n}} \cdot \mathbf{J}^\eta(\mathbf{r})|_{r_1 \rightarrow 0} = 0, \eta = 1, 2, 3$.

Using the definition, Eq. (21), one finds that both the diffusion equation [for this see also Ref.36], Eq. (7), and the boundary conditions, Eq. (19), can be written in terms of the covariant derivative as

$$-i\omega S^\eta + D\mathcal{D}_i^{\eta\eta'} J_i^{\eta'} = 0 \quad (22)$$

$$\hat{\mathbf{n}} \cdot \mathbf{J}^\eta \Big|_{r_1 \rightarrow 0} = 0. \quad (23)$$

Thus, spin diffusion with linear SOI has a (formal) analogy to charge diffusion: In charge diffusion, both the diffusion equation $\dot{\rho} = D\nabla \mathbf{j}$ for the charge density ρ and the BCs $\hat{\mathbf{n}} \cdot \mathbf{j} = 0$ contain the same charge current \mathbf{j} . The current $\mathbf{j} = \nabla \rho$ is given in terms of the spatial derivative of the density. Analogously, the spin current is given as the SU(2)-covariant derivative of S^η .

In Ref. 29, in an attempt to identify a spin current directly from the diffusion equation, Eq. (7) was rewritten (for $\mathbf{b}_0 = 0$) in the form

$$-i\omega S^\eta + [\Gamma(S - S_b)]^\eta - D\nabla \cdot \tilde{\mathbf{J}}^\eta = 0, \quad (24)$$

where the “spin current”

$$\tilde{J}_i^\eta = \frac{\partial}{\partial r_i} \hat{S}^\eta(\mathbf{r}) - 4m\Omega_{ki}\epsilon_{k\eta\eta'} \hat{S}^{\eta'}(\mathbf{r}), \quad (25)$$

however, differs from J_i^η by a relative factor of 2. This discrepancy is resolved when the definitions Eqs. (20), (21) are used making the introduction of two different spin currents J and \tilde{J} unnecessary.

VI. SOLUTIONS OF THE DIFFUSION EQUATION

First, we obtain a solution of Eq. (7) in an infinite sample. In this case the bulk Green's functions $G_b^{R/A}(\mathbf{x}, \mathbf{x}') = G_b^{R/A}(\mathbf{x} - \mathbf{x}')$ are translationally invariant and, thus, $X^{\mu\nu} \equiv \int d^2x' X^{\mu\nu}(\mathbf{r}, \mathbf{x}')$ becomes independent of \mathbf{r} . The spatially uniform ansatz

$$\mathbf{S}_\infty = [\Gamma - i\omega]^{-1} \Gamma \mathbf{S}_b \quad (26)$$

solves both the integral equation [Eq. (5)] and the diffusion equation [Eq. (7)]. The same result for the polarization at finite ω was found in Ref. 50 using a kinetic equation and in Refs. 37,38 in the linear response formalism. Remarkably, \mathbf{S}_∞ is not simply given by the ac internal field $\Omega(\mathbf{p}_d)$ corresponding to ac drift momentum $\mathbf{p}_d = e\mathbf{E}(\omega)\tau/(1 - i\omega\tau)$, but depends on the spin relaxation rate. Therefore, the deviation of \mathbf{S}_∞ from \mathbf{S}_b becomes appreciable already at a relatively small frequency $\omega \simeq \Gamma_{DP}$ rather than at a much higher frequency $\omega \simeq \tau^{-1}$, which marks the dispersion of \mathbf{p}_d . Note also

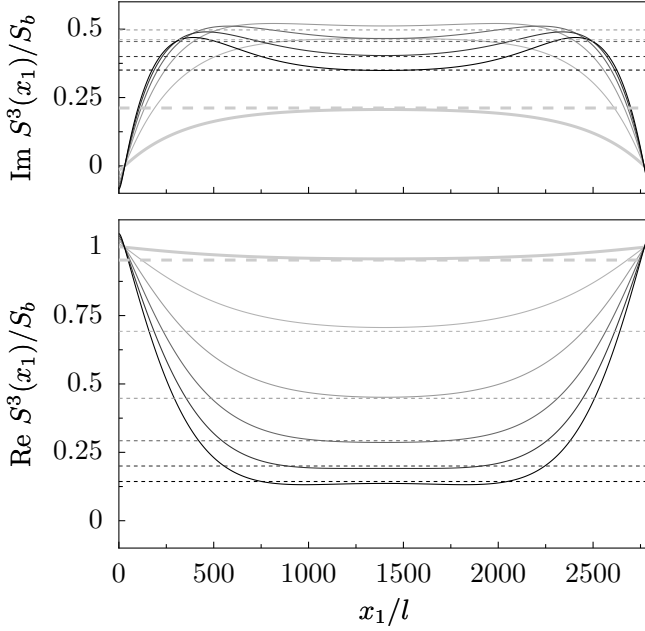


FIG. 4: Real(upper panel) and imaginary parts (lower panel) of the out-of-plane spin polarization $S^3(x)/S_b$ for frequencies $\omega\tau = 0.1, 0.3, 0.5, 0.7, 0.9, 1.1 \times 10^{-5}$ (grey to black lines), $\xi_\beta = 0.1$, $\xi_\alpha = 0.003$, $L = 2800l$, and $S_b = 1\mu\text{m}^{-2}$. The geometry with $\mathbf{E}||[\bar{1}10]$ is shown in Fig. 1 (b). Horizontal dashed lines mark ac bulk polarization according to Eq. (26) for the same parameters.

that there is no dc bulk polarization at $|\alpha| = |\beta|$, if the limit of $\alpha \rightarrow \pm\beta$ is taken before the limit of $\omega \rightarrow 0$ [see Ref. 51 for a discussion of this point].

We now estimate the magnitude of \mathbf{S}_b . We choose parameters similar to the (low-mobility) sample employed in Ref. 3 except for a higher mobility and a lower sheet density. With $\alpha = 1.0 \times 10^{-12}$ eVm, sheet density $n_2 = 1.0 \times 10^{15} \text{ m}^{-2}$, and transport mean free path $\tau = 5 \times 10^{-13}$ s and choosing $E = 5 \text{ mV}/\mu\text{m}$, we obtain the bulk polarization due to Rashba SOI $S_{b,\alpha} \equiv 2\nu e E \tau \alpha = 1.1\mu\text{m}^{-2}$, or about 1 spin per μm^2 ($S_b/n_2 = 0.1\%$). The magnitude of S_∞ and, as we will see below, the magnitude of the spatially non-uniform terms in the solution are proportional to S_b . Depending on the geometry and on whether the Rashba and Dresselhaus SOIs add constructively or destructively, the overall amplitude of the spin oscillations and edge spin accumulation is modified. In case (a) in Fig. 1, one finds $S_b = S_{b,\alpha}(1 + \beta_{[001]}/\alpha)$ while in case (b) $S_b = S_{b,\alpha}(1, 0, \beta_{[110]}/\alpha)$, where $\beta_{[001]}$ and $\beta_{[110]}$ is the Dresselhaus SOI strength in the $[001]$ - and $[110]$ -grown QW, respectively.

We now focus on the position-dependent spin profile in a semiconductor channel of finite width. As before, we assume translational invariance along the channel so that the diffusion equation Eq. (7) becomes an inhomogeneous ordinary differential equation

$$L(\partial_{r_1})[\mathbf{S}(\mathbf{r}_1) - \mathbf{S}_b] = i\omega\tau\mathbf{S}_b \quad (27)$$

in the transverse coordinate r_1 , where the differential operator $L(\partial_{r_1})$ is defined by Eqs. (7) and (27). The solution

$$\mathbf{S} = \mathbf{S}_\infty + c^k \mathbf{s}_k(\mathbf{r}) \quad (28)$$

consists of the uniform part \mathbf{S}_∞ , given by Eq. (26) (inhomogeneous solution), and a linear combination of $k = 1, 2, \dots, 6$ eigenmodes $\mathbf{s}_k = \mathbf{s}_{k,0} e^{\theta_k r_1}$, satisfying $L(\nabla_r)\mathbf{s}(\mathbf{r}) = 0$. The wave numbers $\theta_{1,\dots,6}$ (in arbitrary order) in case (a) are given by⁶⁰

$$\begin{aligned} \theta_{1,2} &= \mp l^{-1} \sqrt{2\tau(\Gamma_+ - i\omega)} \\ \theta_{3,4,(5,6)} &= \frac{+(-)1}{2D} \left[2D(\Gamma_+ - 2i\omega) - C_-^2 \right. \\ &\quad \left. + (-) \mp 2\sqrt{-2D(\Gamma_+ - 2i\omega)C_-^2 + D^2\Gamma_+^2} \right]^{\frac{1}{2}} \end{aligned} \quad (29)$$

Some of θ_k are shown in Fig. 2 as functions of α/β . The real and imaginary part of the wave number are responsible for exponentially growing (decaying) and oscillatory parts of the mode, respectively. The coefficients c^k are determined by the boundary conditions in the form $M\mathbf{c} = -((B-1)(\mathbf{S}_\infty - \mathbf{S}_b), -(B-1)(\mathbf{S}_\infty - \mathbf{S}_b))$ where M is a 6×6 -matrix obtained by inserting the general solution into Eq. (16) [see also Eq. (B3) in Appendix B]. The coefficients c^k determine the magnitude of the non-uniform part of \mathbf{S} , i.e., if all c^k are zero the solution is spatially uniform. Although explicit expressions for c are too lengthy to be displayed here, the scaling of c with ω can be found on general grounds. Indeed, all the entries of the matrix $M^{-1}\text{diag}((B-1), -(B-1))$ are of order 1. The order of magnitude of c_k is thus given by $|\mathbf{S}_\infty - \mathbf{S}_b| \approx (\omega/\Gamma)|\mathbf{S}_b|$, where the latter holds for $\omega \lesssim \Gamma$. The non-uniform part of \mathbf{S} (proportional to the c 's), thus, scales linearly with ω for $\omega \ll \Gamma$ and becomes appreciable at the frequency scale $\omega \simeq \Gamma \ll \tau^{-1}$.

A solution for \mathbf{S} in a $[001]$ -grown QW (Fig. 1 a) is shown in Fig. 3. The electric field \mathbf{E} is along the $[110]$ axis and the strengths of the Rashba and Dresselhaus SOIs are chosen as $\alpha \approx -\beta$, so that the wave numbers (cf. Fig. 2) are almost imaginary. In this case, oscillations of the out-of-plane spin density S^3 extend almost over the entire channel. Simultaneously with α approaching $-\beta$, however, the internal field $\mathbf{\Omega}(e\mathbf{E}\tau) \propto \alpha + \beta$ and, thus, the overall amplitude S_b of the spin density becomes small. In other words, suppression of the damping rate $\text{Re}\theta_i \propto |\alpha + \beta|$ close to the special point $\alpha = -\beta$ competes with a suppression of the overall amplitude, so that a purely oscillatory mode cannot be excited in this geometry.

Figure 4 depicts the polarization profile in a wide $[110]$ -grown QW as shown in Fig. 1 (b), where the bulk polarization (due to the Dresselhaus SOI) is out-of-plane. For a weak Rashba SOI, the wave numbers of the characteristic modes are almost real, i.e., the modes are strongly damped. As a result, the polarization close to the boundary is substantially larger than the bulk value given by Eq. (26).

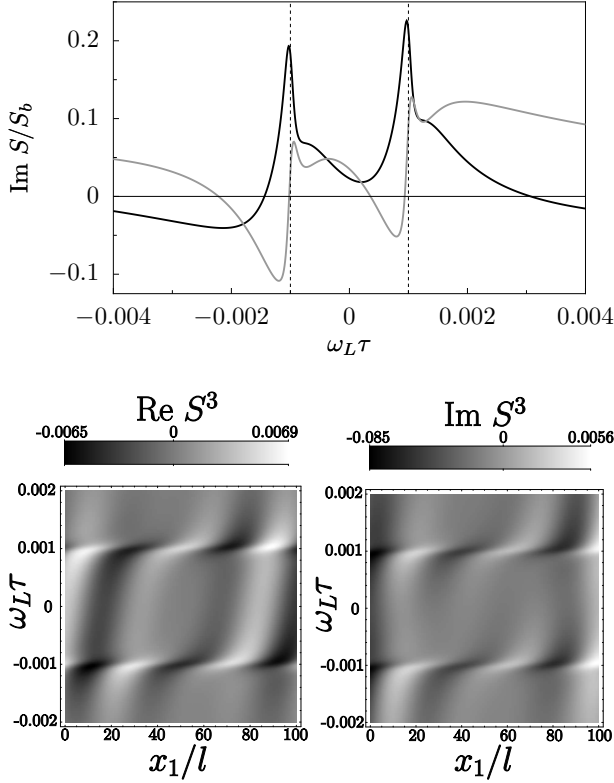


FIG. 5: Polarization in the EDSR geometry $\mathbf{E}, \mathbf{B} \parallel \mathbf{y}$ for case shown in Fig. 1(a) with $\mathbf{S}_b = 0.02 \mu\text{m}^{-2}$. Upper panel: $\text{Im} S^3(x = 20l)$ (black) and $\text{Im} S^1(x = 20l)$ (grey curve) are shown as a function of $\omega_L \tau$. Resonance is seen at $\pm \omega_L \tau = \omega \tau = 10^{-3}$. Parameters of the [001]-grown QW: $\xi_\beta = -0.08$, $\xi_\alpha = 0.1$, $L = 100l$. Lower Panel: Density plot of $\text{Re} S^3(x)$, $\text{Im} S^3(x)$ as a function of x and $\omega_L \tau / \xi_\alpha^2$ for the same parameters.

VII. EDSR AND DRIVEN SPIN HELIX

We now focus on electric-dipole-induced spin resonance (EDSR)^{39,40,41,42,43,37,38,44,45} in the finite Hall bar geometry. We calculate the spin polarization \mathbf{S} due to a simultaneous effect of ac electric field and dc magnetic field \mathbf{b}_0 , both along the channel. The directions of the fields are chosen in such a way so that the internal field $\Omega(e\mathbf{E}(\omega)\tau)$ and \mathbf{b}_0 are perpendicular.⁶¹ This geometry is suitable for an observation of *electrically* driven Rabi oscillations of the spin polarization between the directions along and opposite to \mathbf{b}_0 .^{37,38,40}

We focus on case (a) in Fig. 1. The magnetic field \mathbf{b}_0 leads to an equilibrium polarization (Pauli paramagnetism) $\mathbf{S}_{b_0} \propto \hat{\mathbf{x}}_2 \omega_L = 2\mathbf{b}_0$ in the longitudinal direction of the channel. In addition, the polarization in the bulk of the sample (transverse to \mathbf{b}_0) is modified. In the geometry of Fig. 1 (a) with $\mathbf{b}_0 \parallel \mathbf{e}_{x_2}$, we find for the bulk

polarization

$$\mathbf{S}_\infty = \begin{pmatrix} (\omega_L^2 + \Gamma_-(\Gamma_+ + \Gamma_- - i\omega)) \\ 0 \\ -i\omega\omega_L \end{pmatrix} \times \frac{S_b}{\omega_L^2 - \omega^2 - i\omega(\Gamma_+ + 2\Gamma_-) + \Gamma_-^2 + \Gamma_+\Gamma_-}, \quad (30)$$

where $\Gamma_\pm = 2p_F^2\tau(\alpha \pm \beta)^2$. In the absence of the magnetic field, i.e., for $\omega_L = 0$, Eq. (30) reduces to Eq. (26). Additionally, the characteristic modes change due to \mathbf{b}_0 . The wave numbers θ are determined by the requirement of vanishing eigenvalues

$$\frac{1}{2}\Gamma_+ + \Gamma_- - D\theta^2 - i\omega \mp \frac{1}{2}\sqrt{\Gamma_+^2 - 4(\omega_L - \theta C_-)^2} = 0 \quad (31)$$

of the differential operator $L(\theta)$ defined by Eqs. (7),(27).

We focus on the case of $\alpha \approx -\beta$. Expanding to first order in $\Gamma_+ / (\omega_L - \theta C_-) \ll 1$, one finds

$$\begin{aligned} \theta_{1,2} &= \mp l^{-1} \sqrt{2\tau(\Gamma_+ - i\omega)}, \\ \theta_{3,4} &= \frac{iC_- \mp \sqrt{2}\sqrt{D[\Gamma_+ - 2i(\omega + \omega_L)]}}{2D}, \\ \theta_{5,6} &= \frac{-iC_- \mp \sqrt{2}\sqrt{D[\Gamma_+ - 2i(\omega - \omega_L)]}}{2D}. \end{aligned} \quad (32)$$

At resonance, i.e., for $\omega_L = \omega$, the wave numbers $\theta_{5,6}$ in Eq. (32) become purely imaginary because $\Gamma_+ = 0$ for $\alpha = -\beta$. The modes $s_{5,6}$ are thus completely undamped oscillations of the spin density with wave length $\lambda_{SO}^- = 1/2m(\beta - \alpha)$ [cf. Fig 2]. Note that in the considered case of $\alpha = -\beta$ the Hamiltonian commutes with the longitudinal spin ($[H, \sigma^2] = 0$), i.e., the $U(1)$ -symmetry described in Ref. 32 remains intact; however, the $SU(2)$ -symmetry used in Ref. 21 to demonstrate the existence of the persistent spin helix is broken in the presence of \mathbf{b}_0 .

Figure 5 shows a profile of the spin polarization under EDSR conditions. At resonance ($\omega_L = \pm\omega$), the overall amplitude of the out-of-plane polarization is enhanced. This enhancement becomes particularly strong for $\Gamma_+ \approx 0$ occurring at $\alpha = -\beta$.

Solving the diffusion equation [Eq. (7)] to first order in Γ_+ for the case $\alpha \approx -\beta$, $\omega \approx +\omega_L$, we obtain the following expression for the spin density close to resonance ($\omega \approx +\omega_L$)

$$\begin{aligned} \mathbf{S}(r_1) &\approx \mathbf{S}_\infty + \frac{(S_b^1 - S_\infty^1 - iS_\infty^3)(\xi_\beta - \xi_\alpha)}{\sinh(LR/l)R} \begin{pmatrix} i \\ 0 \\ 1 \end{pmatrix} \\ &\times \left[e^{-ir_1/\lambda_{SO}^-} \cosh(R(L - r_1)/l) - e^{i(L - r_1)/\lambda_{SO}^-} \cosh(Rr_1/l) \right], \end{aligned} \quad (33)$$

where $R = \sqrt{\tau\Gamma_+ - 2i(\omega - \omega_L)\tau}$. Equation (33) describes a spin density wave along the transverse direction of the Hall bar with wave length λ_{SO}^- and an amplitude proportional to $1/\sinh(LR/l)R$. We discuss this result in more detail below. Inserting Eq. (30) for \mathbf{S}_∞ into Eq. (33), setting $\omega = \omega_L$, and expanding the hyperbolic functions in Eq. (33) for a narrow channel with width $L \ll \lambda_{SO}^+ = 1/2m(\alpha + \beta)$, one obtains the dominant α -dependence of \mathbf{S} around the $\alpha \approx -\beta$ point as

$$S^3(r_1) \approx K \frac{\alpha + \beta}{(\xi_\alpha + \xi_\beta)^2 + 2\tau\Gamma^{\text{res}}} \times e^{-ir_1/\lambda_{SO}^-} \left[e^{iL/\lambda_{SO}^-} - 1 \right], \quad (34)$$

where $K = [-i\omega/\Gamma_-](-2\nu eE\tau)(\xi_\beta - \xi_\alpha)l/L$ depends only on the combination $\beta - \alpha$. Here, we introduced a phenomenological linewidth $\Gamma^{\text{res}} = \Gamma_y^{\text{res}} + 2\Gamma_x^{\text{res}} + \mathcal{O}((\omega\tau)^2)$ to model the regularization of the amplitude of S^3 at $\alpha + \beta = 0$, which for $\Gamma^{\text{res}} = 0$ would diverge as $1/(\alpha + \beta)$. For $\alpha + \beta = 0$, the relaxation mechanisms due to linear intrinsic SOIs, which are dominant for generic $\alpha \neq \pm\beta$, are ineffective, and finite spin relaxation rates Γ_x^{res} and Γ_y^{res} of the x_1 and x_2 spin components, respectively, are due to an extrinsic or cubic Dresselhaus SOI.

Equation (34) describes a spin density wave $S^3(r_1)$ at frequency ω with a spatial profile of the form e^{-ir_1/λ_{SO}^-} . The real and imaginary parts of S^3 have stationary nodes separated by the shortest of the two SO lengths, i.e., λ_{SO}^- . In addition, the spin profile is subject to a quantization condition: \mathbf{S} is proportional to a factor $1 - e^{iL/\lambda_{SO}^-}$, which vanishes for $L = 2\pi N\lambda_{SO}^-$ (with N being an integer) and becomes maximal for $L = (2N + 1)\pi\lambda_{SO}^-$. The profile described by Eq. (34) arises due to an excitation of the spin helix modes $s_{5,6}$ under the EDSR conditions. The spatial oscillations of these modes have the same “magic” wave number $\theta = 1/\lambda_{SO}^-$ as the static persistent spin helix.^{21,32} However, whereas the persistent spin helix is time-independent, the spin profiles in Eq. (33),(34) oscillate also in time at each point r_1 with the frequency ω_0 of the applied electric field. [The explicit time-dependence, e.g., $S(r_1, t) \propto \sin(r_1/\lambda_{SO}^- + \omega_0 t)$ for $L = (2N + 1)\pi\lambda_{SO}^-$ and for $\mathbf{E}(t) = \mathbf{E}_0 \cos(\omega_0 t)$, is obtained by inverse Fourier transform of Eqs. (33),(34).]. This driven spin helix is a generalization of a static spin helix structure to the time-dependent case.

Spatial quantization due to the Hall-bar boundaries, moreover, leads to further enhancement of the amplitude of the spin helix modes in the EDSR regime. The amplitude $(\alpha + \beta)/[(\xi_\alpha + \xi_\beta)^2 + 2\tau\Gamma^{\text{res}}]$ is infinite for $\alpha = -\beta$ in a model with strictly linear SOI, i.e. for $\Gamma^{\text{res}} = 0$, but is regularized by the next-to-leading order effects due to cubic Dresselhaus and extrinsic SOIs, giving rise to a finite linewidth Γ^{res} .⁶² Such an enhancement of the amplitude of the driven spin helix close to the $\alpha = -\beta$ point in relatively narrow QWs may be observable, e.g., by optical techniques.^{2,3}

VIII. CONCLUSIONS

In conclusion, we have described several signatures of electrically induced spin polarization and the spin-Hall effect due to *linear* spin-orbit interactions. We have shown that the spin-Hall effect and edge spin accumulation—while being absent for dc electric fields—becomes finite for time-dependent electric fields. In particular, we have found that boundary effects can extend over the whole sample due to driven spin helix modes for the case of the linear Rashba and Dresselhaus spin-orbit interaction being of equal strengths. The amplitude of these helix modes as a function of the spin-orbit interaction strengths is strongly enhanced due to spatial quantization under the conditions of electric-dipole-induced spin resonance.

ACKNOWLEDGMENTS

M.D. and D.L. acknowledge financial support from the Swiss NF and the NCCR Nanoscience Basel. D.L.M. acknowledges support from the Basel QC2 visitor program and NSF-DMR-0908029.

APPENDIX A: SPIN DIFFUSION EQUATION

We start from the impurity averaged Kubo formula (for $E_F\tau \gg 1$) for the spin density

$$S^i(\mathbf{r}) = \left[\text{Diagram 1} + \text{Diagram 2} \right] \frac{e}{2\pi} E_j(\omega) \\ = \frac{e}{2\pi} \int d^2x' \left[\delta^{i\nu} \delta(\mathbf{r} - \mathbf{x}') + \int d^2x 2m\tau X^{i\mu}(\mathbf{r}, \mathbf{x}) D^{\mu\nu}(\mathbf{x}, \mathbf{x}') \right] \gamma^\nu(\mathbf{x}'), \quad (A1)$$

where solid lines denote impurity averaged Green's functions $G_E^{R/A}$ and dashed lines denote correlators of impurity potential.^{37,47,52} The first term of Eq. (A1) is the “bubble” diagram $\gamma^\nu(\mathbf{r}) = \text{tr} \{ \langle \mathbf{r} | \sigma^\nu G_{E_F+\omega}^R \hat{v}_j G_{E_F}^A | \mathbf{r} \rangle \} E_j(\omega)$, i.e., a spin response to the electric field in the absence of vertex corrections. The latter are described by the diffuson $D^{\mu\nu}(\mathbf{r}, \mathbf{x})$, which is defined by the integral equation

$$D^{\mu\nu}(\mathbf{r}, \mathbf{x}') = \frac{\delta^{\mu\nu} \delta(\mathbf{r} - \mathbf{x}')}{2m\tau} + \int d^2y X^{\mu\rho}(\mathbf{r}, \mathbf{y}) D^{\rho\nu}(\mathbf{y}, \mathbf{x}'), \quad (A2)$$

where $X^{\mu\nu}$ is given by Eq. (6). Iterating Eq. (A1) once with the help of Eq. (A2), we find

$$S^i(\mathbf{r}) = \frac{e}{2\pi} (2m\tau) \int d^2x' D^{i\nu}(\mathbf{r}, \mathbf{x}') \gamma^\nu(\mathbf{x}'). \quad (A3)$$

Multiplying Eq. (A2) by $\frac{e}{2\pi}2m\tau\gamma^\nu(\mathbf{x}')$ and integrating over \mathbf{x}' , we obtain the integral equation for the spin density

$$S^i(\mathbf{r}) = \frac{e}{2\pi}\gamma^i(\mathbf{r}) + \int d^2x X^{i\nu}(\mathbf{r}, \mathbf{x})S^\nu(\mathbf{x}), \quad (\text{A4})$$

which can be further simplified by partially evaluating the “bubble” term $\gamma^i(\mathbf{r})$ in Eq. (A4). We define the spin-momentum correlation functions³⁷

$$Y^{\eta j}(\mathbf{r}) = \int \frac{d^2x}{2m\tau} \text{tr} \left\{ \sigma^\eta G^R(\mathbf{r}, \mathbf{x}) \frac{-i\partial}{m\partial x_j} G^A(\mathbf{x}, \mathbf{r}) \right\} \quad (\text{A5})$$

$$Y_b^{\eta j} = -\frac{\Omega_{\eta j}}{1 - i\omega\tau} \approx -(1 + i\omega\tau)\Omega_{\eta j}, \quad (\text{A6})$$

where Eq. (A6) is obtained by evaluating Eq. (A5) using the bulk Green’s functions of an infinite sample. Inserting the definition of the velocity operator $\hat{v}_j = \frac{\hat{p}_j}{m} + \Omega_{kj}\sigma^k$, we obtain $(e/2\pi)\gamma^i(\mathbf{r}) = -\int d^2x X^{ik}(\mathbf{r}, \mathbf{x})S_b^k + 2m\tau(e/2\pi)Y^{ij}(\mathbf{r})E_j$. We can rewrite Eq. (A4) as

$$S^i(\mathbf{r}) - S_b^i = i\omega\tau S_b^i + \int d^2x X^{ij}(\mathbf{r}, \mathbf{x})(S^j(\mathbf{x}) - S_b^j) + [Y(\mathbf{r}) - Y_b]^{ij} 2\nu e E_j \tau. \quad (\text{A7})$$

From now on, we treat the regions close to the boundary and in the bulk separately. In the bulk, one obviously has $[Y(\mathbf{r}) - Y_b] = 0$ and arrives thus at Eq. (5). At the boundary, the Green’s functions $G_0^{R/A} = G_{b,0}^{R/A} - G_{b,0}^{*R/A}$ constructed in Sec. V have to be used to evaluate $\gamma^i(\mathbf{r})$, $Y^{\mu\mu}(\mathbf{r})$. Neglecting terms oscillating with a period of $1/p_F$, as described in Sec. IV, one finds that $Y^{ij}(\mathbf{r})E_j = Y_b^{ij}E_j$ to linear order in the SOL. Therefore, the last term in Eq. (A7) vanishes. Consequently, Eq. (A7) turns into Eq. (5) and can be used for the derivation of both the bulk diffusion equation and the boundary conditions.

APPENDIX B: BOUNDARY CONDITIONS

For the coefficients B and C in Eq. (16) describing a boundary with normal vector $\hat{\mathbf{n}}$, we found

$$\delta B^{\mu\nu}(\hat{\mathbf{n}}) \equiv [B - \mathbb{1}]^{\mu\nu} = -\frac{2}{\pi} 2p_F \tau \Omega^m(\mathbf{n}) \epsilon_{m\nu\mu}, \quad (\text{B1})$$

$$C_j^{\mu\nu}(\hat{\mathbf{n}}) = \frac{2}{\pi} \delta^{\mu\nu} l \hat{\mathbf{n}} \cdot \mathbf{e}_j, \quad (\text{B2})$$

where we neglected terms proportional to $\omega\tau \ll 1$. We define a 6×6 matrix

$$M = \begin{pmatrix} (\delta B(\hat{\mathbf{n}}) + \theta_1 C(\hat{\mathbf{n}})) \mathbf{s}_{1,0} e^{\theta_1 r} \Big|_{r=0} & (\delta B(\hat{\mathbf{n}}) + \theta_2 C(\hat{\mathbf{n}})) \mathbf{s}_{2,0} e^{\theta_2 r} \Big|_{r=0} & \dots & (\delta B(\hat{\mathbf{n}}) + \theta_6 C(\hat{\mathbf{n}})) \mathbf{s}_{6,0} e^{\theta_6 r} \Big|_{r=0} \\ (\delta B(-\hat{\mathbf{n}}) + \theta_1 C(-\hat{\mathbf{n}})) \mathbf{s}_{1,0} e^{\theta_1 r} \Big|_{r=L} & (\delta B(-\hat{\mathbf{n}}) + \theta_2 C(-\hat{\mathbf{n}})) \mathbf{s}_{2,0} e^{\theta_2 r} \Big|_{r=L} & \dots & (\delta B(-\hat{\mathbf{n}}) + \theta_6 C(-\hat{\mathbf{n}})) \mathbf{s}_{6,0} e^{\theta_6 r} \Big|_{r=L} \end{pmatrix} \quad (\text{B3})$$

and a vector $\mathbf{A} = (\mathbf{A}_0, \mathbf{A}_L)$, where $\mathbf{A}_{0,L} = \delta B(\pm\hat{\mathbf{n}})(\mathbf{S}_\infty - \mathbf{S}_b)$. Inserting the general solution $\mathbf{S} =$

$\mathbf{S}_\infty + c_k \mathbf{s}_{0,k} e^{\theta_k r_1}$ into Eq. (16), the BCs can be rewritten as $M\mathbf{c} = -\mathbf{A}$.

- ¹ M. I. D’yakonov and M. I. Perel, JETP Lett. **13**, 467 (1971).
- ² Y. K. Kato, R. C. Myers, A. C. Gossard, and D. D. Awschalom, Science **306**, 1910 (2004).
- ³ V. Sih, R. C. Myers, Y. K. Kato, W. H. Lau, A. C. Gossard, and D. D. Awschalom, Nature Physics **1**, 31 (2005).
- ⁴ H.-A. Engel, E. I. Rashba, and B. I. Halperin, in *Handbook of Magnetism and Advanced Magnetic Materials* (John Wiley & Sons Ltd, 2007).
- ⁵ L. S. Levitov, Y. V. Nazarov, and G. M. Eliashberg, Zh. Eksp. Teor. Fiz. **88**, 229 (1985).
- ⁶ V. M. Edelstein, Solid State Comm. **73**, 233 (1990).
- ⁷ Y. K. Kato, R. C. Myers, A. C. Gossard, and D. D. Awschalom, Appl. Phys. Lett. **87**, 022503 (2005).
- ⁸ D. D. Awschalom, D. Loss, and N. Samarth, eds., *Semiconductor Spintronics and Quantum Computation* (Springer, Berlin, 2002).
- ⁹ J. Wunderlich, B. Kaestner, J. Sinova, and T. Jungwirth,

- Phys. Rev. Lett. **94**, 047204 (2005).
- ¹⁰ J. Sinova, D. Culcer, Q. Niu, N. A. Sinitsyn, T. Jungwirth, and A. H. MacDonald, Phys. Rev. Lett. **92**, 126603 (2004).
- ¹¹ E. I. Rashba, Phys. Rev. B **68**, 241315(R) (2003).
- ¹² S. I. Erlingsson, J. Schliemann, and D. Loss, Phys. Rev. B **71**, 035319 (2005).
- ¹³ O. Chalaev and D. Loss, Phys. Rev. B **71**, 245318 (2005).
- ¹⁴ J. Inoue, G. E. W. Bauer, and L. W. Molenkamp, Phys. Rev. B **70**, 041303(R) (2004).
- ¹⁵ R. Raimondi and P. Schwab, Phys. Rev. B **71**, 033311 (2005).
- ¹⁶ O. V. Dimitrova, Phys. Rev. B **71**, 245327 (2005).
- ¹⁷ I. Adagideli and G. E. W. Bauer, Phys. Rev. Lett. **95**, 256602 (2005).
- ¹⁸ A. G. Mal’shukov, L. Y. Wang, C. S. Chu, and K. A. Chao, Phys. Rev. Lett. **95**, 146601 (2005).
- ¹⁹ V. M. Galitski, A. A. Burkov, and S. DasSarma, Phys. Rev. B **74**, 115331 (2006).

- ²⁰ E. G. Mishchenko, A. V. Shytov, and B. I. Halperin, Phys. Rev. Lett. **93**, 226602 (2004).
- ²¹ B. A. Bernevig, J. Orenstein, and S.-C. Zhang, Phys. Rev. Lett. **97**, 236601 (2006).
- ²² Y. Tserkovnyak, B. I. Halperin, A. A. Kovalev, and A. Brataas, Phys. Rev. B **76**, 085319 (2007).
- ²³ A. A. Burkov, A. S. Núñez, and A. H. MacDonald, Phys. Rev. B **70**, 155308 (2004).
- ²⁴ I. Adagideli, M. Scheid, M. Wimmer, G. E. W. Bauer, and K. Richter, N. J. Phys. **9**, 382 (2007).
- ²⁵ A. Shnirman and I. Martin, Europhys. Lett. **78**, 27001 (2007).
- ²⁶ Y. V. Pershin, Physica E **27**, 77 (2005).
- ²⁷ T. D. Stanescu and V. Galitski, Phys. Rev. B **75**, 125307 (2007).
- ²⁸ E. I. Rashba, Physica E **34**, 31 (2006).
- ²⁹ O. Bleibaum, Phys. Rev. B **74**, 113309 (2006).
- ³⁰ R. Raimondi, C. Gorini, M. Dzierzawa, and P. Schwab, Solid State Comm. **144**, 524 (2007).
- ³¹ N. P. Stern, D. W. Steuermann, S. Mack, A. C. Gossard, and D. D. Awschalom, Nature Physics **4**, 843 (2008).
- ³² J. Schliemann, J. C. Egues, and D. Loss, Phys. Rev. Lett. **90**, 146801 (2003).
- ³³ J. D. Koralek, C. P. Weber, J. Orenstein, B. A. Bernevig, S.-C. Zhang, S. Mack, and D. D. Awschalom, Nature **458**, 610 (2009).
- ³⁴ V. A. Zyuzin, P. G. Silvestrov, and E. G. Mishchenko, Phys. Rev. Lett. **99**, 106601 (2007).
- ³⁵ H.-A. Engel, B. I. Halperin, and E. I. Rashba, Phys. Rev. Lett. **95**, 166605 (2005).
- ³⁶ R. Raimondi and P. Schwab, Eur. Phys. Lett. **87**, 37008 (2009).
- ³⁷ M. Duckheim and D. Loss, Nature Physics **2**, 195 (2006).
- ³⁸ M. Duckheim and D. Loss, Phys. Rev. B **75**, 201305(R) (2007).
- ³⁹ R. L. Bell, Phys. Rev. Lett. **9**, 52 (1962).
- ⁴⁰ E. I. Rashba and A. L. Efros, App. Phys. Lett. **83**, 5295 (2003).
- ⁴¹ E. I. Rashba and V. I. Sheka, in *Landau level spectroscopy*, edited by G. Landwehr and E. I. Rashba (North-Holland, Amsterdam, 1991), p. 131.
- ⁴² Y. K. Kato, R. C. Myers, A. C. Gossard, and D. D. Awschalom, Nature **427**, 50 (2004).
- ⁴³ M. Schulte, J. G. S. Lok, G. Denninger, and W. Dietsche, Phys. Rev. Lett. **94**, 137601 (2005).
- ⁴⁴ Z. Wilamowski, H. Malissa, F. Schäffler, and W. Jantsch, Phys. Rev. Lett. **98**, 187203 (2007).
- ⁴⁵ L. Meier, G. Salis, I. Shorubalko, E. Gini, S. Schön, and K. Ensslin, Nature Phys. **3**, 650 (2007).
- ⁴⁶ R. Winkler, *Spin-orbit Coupling Effects in Two-Dimensional Electron and Hole Systems* (Springer, 2003).
- ⁴⁷ E. Akkermans and G. Montambaux, *Mesoscopic physics of electrons and photons* (Cambridge University Press, 2007).
- ⁴⁸ J. Rammer and H. Smith, Rev. Mod. Phys. **58**, 323 (1986).
- ⁴⁹ I. V. Tokatly, Phys. Rev. Lett. **101**, 106601 (2008).
- ⁵⁰ O. E. Raichev, Phys. Rev. B **75**, 205340 (2007).
- ⁵¹ M. Duckheim, D. Loss, M. Scheid, K. Richter, İnanc Adagideli, and P. Jacquod, (unpublished) (2009).
- ⁵² O. Chalaev and D. Loss, Phys. Rev. B **80**, 035305 (2009).
- ⁵³ M. Lee, M. O. Hachiya, E. Bernardes, J. C. Egues, and D. Loss, Phys. Rev. B **80**, 155314 (2009).
- ⁵⁴ M. Duckheim and D. Loss, Phys. Rev. Lett. **101**, 226602 (2008).
- ⁵⁵ J. H. Bardarson, I. Adagideli, and P. Jacquod, Phys. Rev. Lett. **98**, 196601 (2007).
- ⁵⁶ I. Adagideli, J. H. Bardarson, and P. Jacquod, J. Phys. **21**, 155503 (2009).
- ⁵⁷ P. G. Silvestrov, V. A. Zyuzin, and E. G. Mishchenko, Phys. Rev. Lett. **102**, 196802 (2009).
- ⁵⁸ In quantum wells with more than one subband the spin-Hall current can be nonzero. See Ref.53.
- ⁵⁹ Qualitatively different spin effects occur in systems with orbital phase coherence, i.e., in mesoscopic disordered⁵⁴ or ballistic systems^{55,56} and on length scales smaller than the mean free path at ballistic boundaries.⁵⁷
- ⁶⁰ Below, we focus on the behavior of S for $\alpha \approx +\beta$ ($\alpha \approx -\beta$). In a [110]-grown quantum well, similar behavior can be found when the Rashba SOI strength is close to zero and the electric field is taken along the $\bar{[110]}$ -direction (the [001]-direction). Therefore, we discuss case (a) in more detail.
- ⁶¹ We also studied the Hanle geometry when $\Omega(e\mathbf{E}(\omega)\tau)||\mathbf{b}_0$; however, the effect of b_0 becomes appreciable only for fields as large as $b_0 \approx \tau^{-1}$ in that case.
- ⁶² A similar regularization from effects outside the linear model occurs for the lifetime of the static spin helix²¹. See Ref. 27.